When Gold Is Not Noble: Nanoscale Gold Catalysts

A. Sanchez,[†] S. Abbet,[†] U. Heiz,[†] W.-D. Schneider,[†] H. Häkkinen,[‡] R. N. Barnett,[‡] and Uzi Landman*[,‡]

Université de Lausanne, Institut de Physique de la Matière Condensée CH-1015 Lausanne, Switzerland, and Georgia Institute of Technology, School of Physics, Atlanta, Georgia 30332-0430

Received: October 8, 1999

While inert as bulk material, nanoscale gold particles dispersed on oxide supports exhibit a remarkable catalytic activity. Temperature-programmed reaction studies of the catalyzed combustion of CO on size-selected small monodispersed Au_n ($n \leq 20$) gold clusters supported on magnesia, and first-principle simulations, reveal the microscopic origins of the observed unusual catalytic activity, with Au_8 found to be the smallest catalytically active size. Partial electron transfer from the surface to the gold cluster and oxygen-vacancy F-center defects are shown to play an essential role in the activation of nanosize gold clusters as catalysts for the combustion reaction.

Introduction

Investigations of reactions heterogeneously catalyzed by metals and alloys are a major area of research endeavors.[1] Here we focus on a class of catalysts which led recently to remarkable and rather surprising findings. In contrast to the inert nature of gold as bulk material,[2] nanosize particles of gold supported on various oxides,[3−5] as well as two-monolayer-thick gold islands of up to 4 nm diameter on titania,[6] were found to exhibit an enhanced catalytic activity, in particular for the low-temperature oxidation of CO.[3,5,6] While the novel heterogeneous catalysis by nanosize gold aggregates supported on oxides is of great significance in current and future environmental, sensor, and chemical technologies,[3] the processes underlying the catalytic activity of gold in reduced dimensions and the reaction mechanisms are not yet understood. In this study we address these issues through investigations of the low-temperature combustion of CO on size-selected gold clusters, Au_n ($n \leq 20$), supported on defect-poor and defect-rich MgO (100) films, demonstrating the size dependence of the activity of nanoscale gold clusters, with Au_8 found to be the smallest size to catalyze the reaction, and revealing that charging of the cluster via (partial) electron transfer from the oxide support, as well as the presence of oxygen- vacancy (F-center) defects in the substrate, play an essential role in the activation of nanosize gold model catalysts.

Catalyst Preparation and Structure

Monodispersed cluster ions, selected from a distribution of cluster sizes obtained via supersonic expansion of a cold (40 K) laser-generated metal plasma, were deposited with low kinetic energy (<0.2 eV/atom) on well-defined oxide surfaces;[7] under these conditions the clusters soft-land (that is, without fragmentation and significant structural distortion) on the substrate.[7−9] Deposition of less than 1% of a monolayer (1 ML $= 2.2 \times 10^{15}$ clusters/cm^2) at a substrate temperature of 90 K assures isolated supported clusters and prevents agglomeration.[10−12] The magnesium oxide supports were prepared in situ by epitaxially growing thin films on a Mo (100) surface.[13] Different annealing temperatures result in defect-poor (1100 K) and defect-rich (840 K) MgO (100) thin films, and the defect densities (which we attribute mainly to oxygen-vacancy F-centers (FC)) were estimated by titration with NO (see upper spectra in Figure 1d,e).[14]

Equilibrium structures of Au_8 clusters adsorbed on MgO (100) were investigated with ab initio simulations.[15,16] for both a defect-free surface and for one containing an FC, MgO (FC). The energy-optimal structure of a gold octamer adsorbed on MgO (FC) shown in Figure 2a,b was obtained through energy minimization via unconstrained structural relaxations of both the cluster and substrate ions, starting from the equilibrium geometry of a free Au_8 cluster deposited on the surface (thus modeling the soft-landing process) in the vicinity of the FC defect. The doubly-occupied FC orbital of the bare surface, whose energy lies in the band-gap of the MgO (100) spectrum split by 2.45 eV from the O (2p)-derived band, is shown in Figure 2c exhibiting an expanded electron distribution above the surface plane localized about the oxygen vacancy.

The binding energy of the cluster in the optimal adsorption geometry[17] (Figure 2a,b) to the surface is rather high (5.56 eV), and the adsorption process is accompanied by charge transfer of ∼0.5 e into the cluster as shown in Figure 2d,e. Similar (partial) charging of the cluster occurs also for adsorption of the gold octamer on a defect-free MgO (100) surface, with only a minor deformation of the cluster from its gas-phase structure, but the binding energy to the surface is reduced by ∼2.2 eV from the MgO (FC)/Au_8 case. We remark here that the charging of the adsorbed gold clusters is expected to be most significant for their size-selective catalytic activity in light of (i) the enhanced binding of Au_8 clusters to the MgO (FC) surface which anchors and localizes them near the defect sites, thus reducing their propensity for agglomeration, and (ii) early investigations of molecular oxygen adsorption on (free) gas-phase gold clusters, where only even numbered *anionic* clusters (Au_{2n}^-, $2 \leq n \leq 10$) were found to react with gaseous O_2 molecules with the reactivity correlating with the size-dependent pattern of the electron affinities of the gold clusters.[18] This implies that the oxide surface is indeed essential for the (electronic) catalytic

* Author to whom correspondence should be addressed.
[†] Université de Lausanne.
[‡] Georgia Institute of Technology.

10.1021/jp9935992 CCC: $18.00
Published on Web 11/09/1999

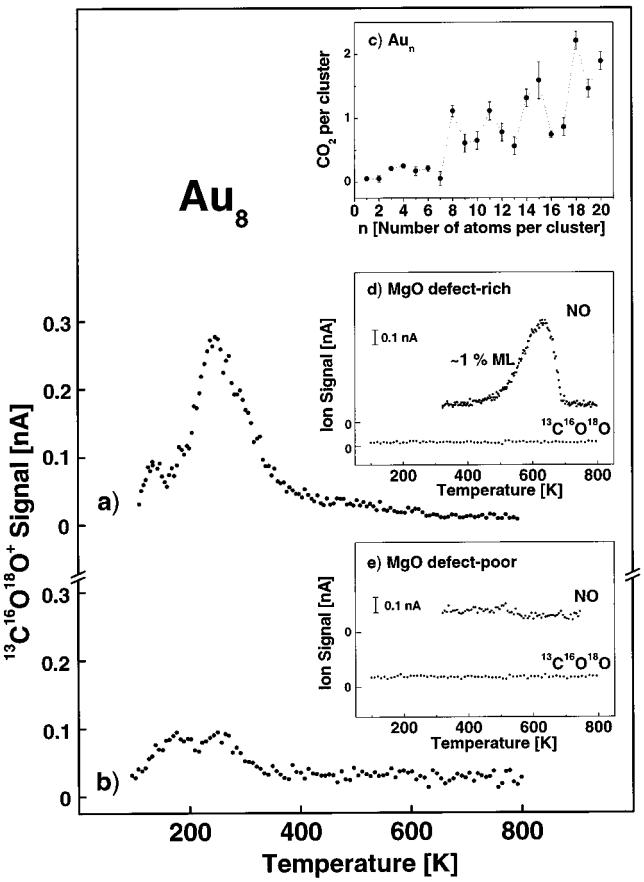

Figure 1. CO combustion on Au_8 (0.4% ML) supported on defect-rich (a) and defect-poor (b) MgO (100) films shown by the production of $^{13}C^{16}O^{18}O$ obtained by TPR experiments. MgO (100)/Au_8 is exposed at 90 K first to an average of 20 molecules of $^{18}O_2$ and subsequently to 20 molecules of $^{13}C^{16}O$ per deposited Au atom; these exposures correspond to saturation as the CO_2 production did not enhance at higher exposures. (c) Size-dependent overall reactivity of gold clusters, Au_n, supported on defect-rich MgO(100) films, expressed as the number of CO_2 molecules per cluster. Note that clusters up to the heptamer are inert (reactivity < 0.2). (d,e) Results of the titration of NO from defect-rich (d) and defect-poor (e) films (without gold clusters). Note that no CO_2 is formed on both films (lower spectra in each panel) under the same experimental conditions as used for the deposited-cluster experiments.

activity of the supported gold clusters, beyond serving merely as a substrate for dispersing the metal particles.

Catalyzed Oxidation Reactions and Mechanisms

Subsequent to verification that oxidation of CO does not occur on bare MgO substrate films (with and without defects), see lower spectra in Figure 1d,e, the catalyzed combustion of CO by nanosize gold clusters Au_n ($1 \le n \le 20$) adsorbed on the two different MgO films was studied by temperature-programmed reaction (TPR) experiments. Isotopically labeled $^{18}O_2$ and ^{13}CO were used to disentangle the CO_2 production on the cluster from an eventual catalytic oxidation of CO involving oxygen atoms from the MgO substrate. Indeed, the ^{13}CO molecule is exclusively oxidized by $^{18}O_2$ since only the $^{13}C^{16}O^{18}O$ isotopomer is detected. Furthermore, the experiments revealed that the gold clusters up to the heptamer are inert for the oxidation of CO (see Figure 1c) and that the low-temperature (T < 250 K) combustion of CO is most effective for Au_8. Consequently, we set out to elucidate experimentally and theoretically the oxidation of CO by gold octamers supported on magnesia.

The catalytic activity (measured via the amount of desorbed carbon dioxide) on Au_8 (0.4% ML) clusters deposited on defect-poor MgO (100) films observed during one heating cycle (Figure 1b), reveals a very small combustion of CO at temperatures between 150 and 250 K. Surprisingly, CO combustion on Au_8 dramatically increases when depositing the octamer (0.4% ML) on defect-rich MgO-films (see Figure 1a). This particular behavior pertains even after several reaction cycles up to temperatures of 350 K, indicating that the model catalyst is thermally stable. This is further supported by infrared studies, with the vibrational frequencies of ^{13}CO adsorbed on Au_8 (at 90 K before and after annealing to 350 K, and with no oxygen present) showing no change in frequency and integrated absorption intensity (note here that for small metal clusters the vibrational frequency and linewidth of adsorbed CO are rather sensitive to the size and structure of the cluster). In the absence of oxygen, CO desorbs from the supported Au_8 cluster between 150 and 180 K. The catalytically formed $^{13}C^{16}O^{18}O$ desorbs already at 140 K with the main desorption peak at 240 K (Figure 1a). Evaluating the area of the TPR signal in Figure 1a yields the production of about one CO_2 molecule per Au_8 cluster.[11,12]

Each cluster size (Au_n with $1 \le n \le 20$) supported on defect-rich MgO (100) films reveals a distinctly different reactivity, with Au_8 being the smallest cluster size active for the combustion of CO (see Figure 1c). For all active cluster sizes we observed in addition to the relatively small desorption at 140 K a higher temperature channel with a transition from a narrow desorption maximum at 240 K for Au_8 (see Figure 1a) to a broad maximum at 500 K (FWHM = 150 K) for Au_{20}.[19]

To explore the energetics and reaction mechanisms underlying the above observations we performed extensive ab initio simulations,[15] summarized in Figure 3 where we display atomic configurations corresponding to various reaction paths of the oxidation of CO catalyzed by Au_8 clusters adsorbed on MgO (FC). Both O_2 and CO adsorb on the Au_8 cluster supported on the MgO (100) surface (with or without FC defects). However, the observed single sharply peaked stretch frequency of adsorbed CO with $\nu_a = 2102$ cm^{-1} compared to $\nu_a = 2143$ cm^{-1} for the free $^{12}C^{16}O$ molecule, implies a single adsorption site on the cluster and a rather minor influence of adsorption on the internal structure and bonding of the molecule. Indeed, we found that in the optimal adsorption configuration CO binds on-top of an Au atom of the upper triangular facet of the adsorbed Au_8 cluster (see Figure 3d−g) with d(CO) = 1.14 Å (compared to 1.13 Å in the free molecule) and d(AuC) = 1.92 Å.

On the other hand, an O_2 molecule may readily adsorb at several sites, both on the upper Au_8 facet and at the interface between the adsorbed gold cluster and the underlying magnesia surface, and in all cases the adsorbed molecule is found to be activated to a peroxo O_2* molecular state[20,21] with a weakened highly stretched intramolecular bond length (1.41−1.46 Å) compared to that in the free molecule (1.24 Å). On the Au_8 triangular top-facet the most stable molecular adsorption configurations are (i) an edge-top (ET) configuration, with an adsorption energy $E_a = 1.22$ eV (see oxygen atoms marked O_1 and O_2 in Figure 3a,b), and (ii) an edge (E) configuration with $E_a = 0.88$ eV (see Figure 3d,e). Upon coadsorption of CO and O_2 the latter is found in the E adsorption configuration (Figure 3d,e). Another molecular oxygen adsorption site which we consider is the Au_8 cluster periphery at the interface with the MgO surface. Here the molecule adsorbs with the two oxygens lying above an Au−Au bridge of the Au_8 interfacial layer (see Figure 3f,g), and the absorption energies are $E_a = 1.05$ eV and 1.85 eV to MgO(FC)/Au_8 and MgO/Au_8, respectively, with

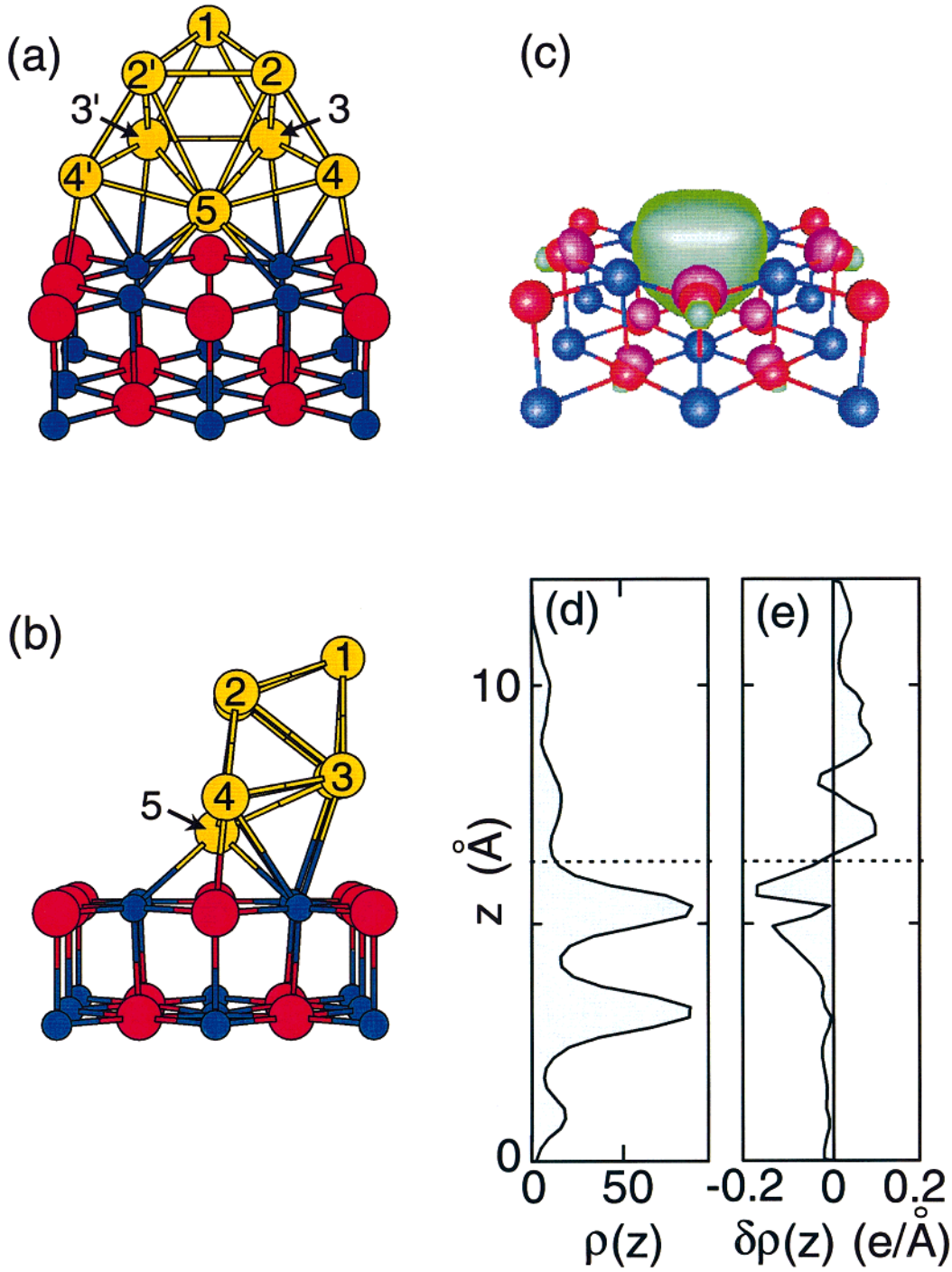

Figure 2. (a,b) Two views of the energy-optimal structure of Au_8 adsorbed on the MgO (100) surface containing an oxygen-vacancy F-center (FC). In (a) the C_{2v} plane of the Au_8 cluster is normal to the page, and in (b) it is parallel to the page. The configuration in (a) is tilted forward by 20° about the horizontal axis to expose the (100) plane of the MgO surface. The FC is in the middle of the top layer of the MgO surface under the Au atom marked 5. The structure of the adsorbed Au_8 cluster may be described as a deformed piece of an hexagonal close-packed crystal with stacked five (bottom)- and three (top)-atom layers. Red, blue, and yellow (numbered) spheres depict O, Mg, and Au atoms, respectively. Here, and in the following (including Figure 3) only a portion of the MgO surface used in the calculations is shown. (c) Isovalue surface of the $2e^-$ FC wavefunction. The selected surface encloses about 50% of the orbital charge, and the sign of the wavefunction is color coded: (+) in green, and (−) in purple. Red and blue spheres depict O and Mg ions. (d) Total valence electron distribution $\rho(z)$ across the slab (in the direction of surface normal). (e) Accumulation ($\delta\rho > 0$) and deficit ($\delta\rho < 0$) of electronic charge, obtained as $\delta\rho(z) = \rho(z) - [\tilde{\rho}(z;Au_8) + \tilde{\rho}(z;\text{substrate})]$, where $\tilde{\rho}(z;Au_8)$ and $\tilde{\rho}(z;\text{substrate})$ are the isolated subsystem densities calculated with atoms in the positions of the fully optimized system. The dotted line denotes the midpoint in the z-direction, $\bar{z}$, between the surface plane and the Au atom (marked 5 in a and b) adsorbed 1.57 Å above the color center. Integrating $\delta\rho(z)$ from the bottom of the substrate to $\bar{z}$ yields transfer of $\delta_e \sim 0.5$ e from the magnesia surface to the gold octamer; this result is rather insensitive to physically reasonable variations in the upper integration limit (for example when taken at $\bar{z} \pm 0.4$ Å we obtain $\delta_e = 0.45$e).

preadsorbed CO. The activation of the adsorbed oxygen molecule involves occupation of the antibonding $\pi_{||}$* molecular orbital (i.e., the molecular oxygen π_g* orbital oriented parallel to the adsorbing surface) which hybridizes with the orbitals of neighboring gold atoms of the partially negatively charged adsorbed gold cluster (Figure 3a).

Reaction Mechanisms. Starting from the optimal ET configuration of O_2* adsorbed on the MgO(FC)/Au_8 catalyst, a gas-

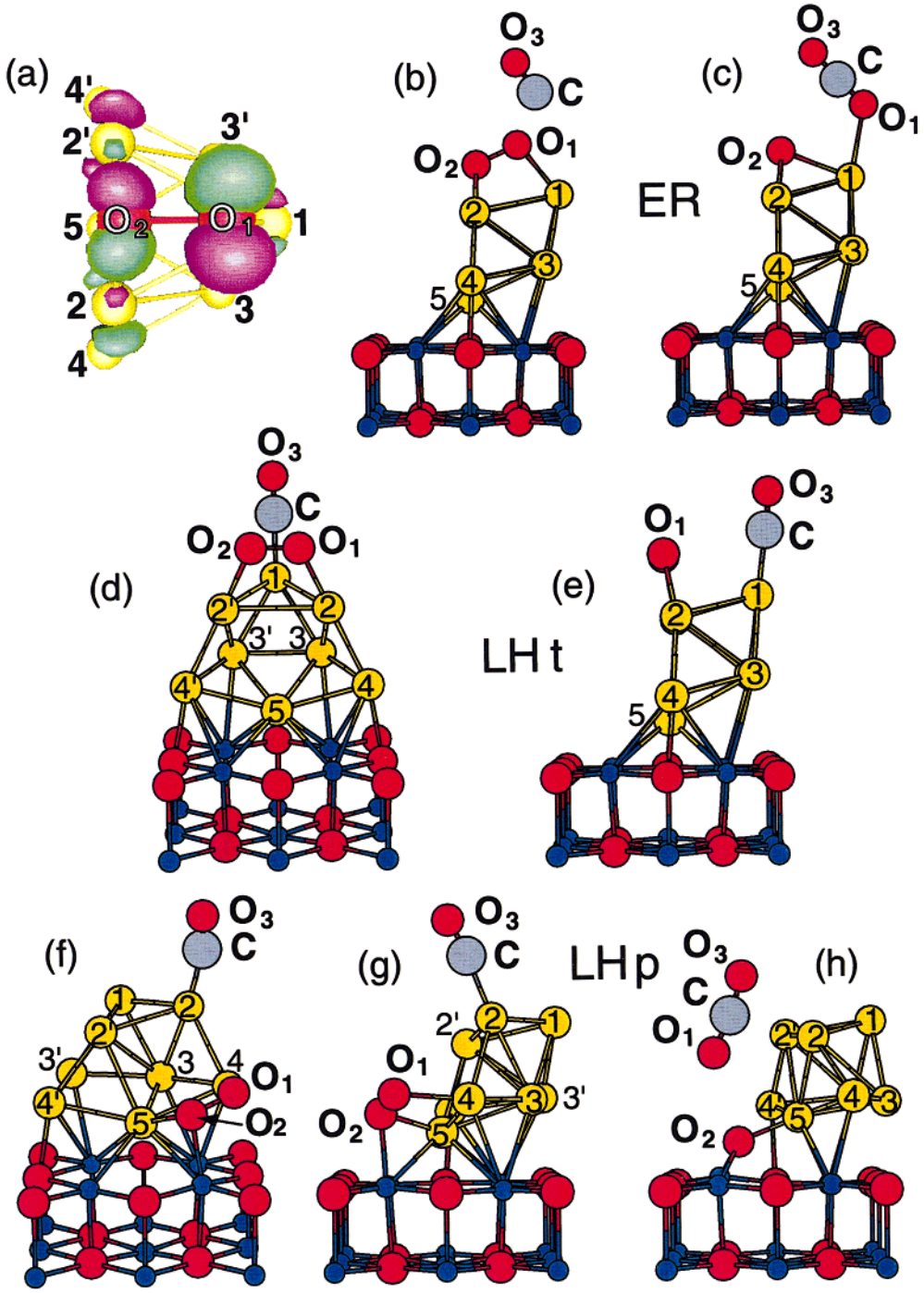

Figure 3. (a) Top view of the isovalue surface of the highest occupied antibonding molecular-orbital (HOMO) $\pi_{\parallel}$* of the oxygen molecule adsorbed in the peraxo ET configuration on the top-facet of the Au_8 cluster supported on the MgO (FC) surface. The wave function is color coded with green (+) and purple (−). The selected isovalue surface encloses 50% of the orbital charge. The locations of the underlying atoms of the Au_8 cluster are depicted by the yellow spheres numbered as in Figure 2a. The locations of the oxygen atoms of the peroxo oxygen molecule are given by the red spheres marked O_1 and O_2. The occupied state next to the HOMO is an antibonding $\pi_{\perp}$* orbital with the p-like lobes perpendicular to the plane (not shown). (b,c) The (direct) ER-type reaction mechanism: (b) snap-shot of the CO molecule (the carbon is colored in light-blue and the oxygen, numbered O_3, in red) approaching the adsorbed peroxo molecule (red spheres marked O_1 and O_2). The Au_8 cluster and underlying portion of the MgO (FC) surface as in Figure 2b; the reaction products consist of a weakly adsorbed carbon dioxide molecule (marked CO_1O_3), and an oxygen atom (marked O_2). (d,e) Two views of the initial configuration for the LHt reaction. The peroxo oxygen molecule (red spheres numbered O_1 and O_2) is adsorbed on top of the Au_8 cluster in an E configuration, and the CO molecule is coadsorbed on top of an Au atom (numbered 1). The reaction product is the same as that shown in (c). (f−h) The LHp reaction mechanism. In (f) and (g) we show two views of the initial configuration with the CO molecule adsorbed on top of the Au_8 cluster and the peroxo oxygen molecule (red spheres numbered O_1 and O_2) coadsorbed on the Au_5−Au_4 bridge at the interfacial periphery of the gold octamer. The reaction products consist of a carbon dioxide molecule (marked O_1CO_3 in (h)) weakly bound to the gold cluster and an adsorbed oxygen (red sphere numbered O_2).

phase CO molecule brought to the vicinity of the peroxo molecule (Figure 3b) reacts spontaneously (*without* an energy barrier) forming a carbon dioxide molecule (the molecule marked O_1CO_3 in Figure 3c) weakly bound to the catalyst (∼0.2 eV); the total exothermicity of the reaction MgO (FC)/Au_8 + O_2(g) + CO(g) → MgO (FC)/Au_8O (CO_2(a)) is ∼4.8 eV and it

is ~5 eV when the CO_2 product is desorbed,[22] here (g) and (a) denote gas-phase and adsorbed molecules, respectively. This Eley−Rideal (ER)-type reaction mechanism corresponds to a low-temperature generation of (weakly adsorbed) CO_2 through direct reaction of gaseous CO with a preadsorbed peroxo O_2* molecule. This reaction channel can occur even at 90 K (that is, during the initial dosing stage in the experiment) with the weakly adsorbed CO_2 product desorbing upon slight heating, correlating with the observed CO_2 desorption peak at 140 K. Another reaction pathway which may contribute to the low-temperature oxidation of CO is of the Langmuir−Hinshelwood (LH) type, where the two reactants are initially coadsorbed on the top-facet of the Au_8 cluster, with the distance between the carbon atom and one of the peroxo oxygens in this local minimum state equal to 3.11 Å ($d(CO_1)$ in Figure 3d,e); in the following we refer to the LH top-facet reaction mechanism as LHt. Through mapping of the potential energy surface along the $C-O_1$ reaction coordinate (via total relaxation of the system with the variable $C-O_1$ distance as a constraint) we determined a rather low energy barrier ΔE_b (LHt) = 0.1 eV (occurring at $d_b(CO_1) \approx 2.0$ Å) for the LHT oxidation channel with the same end product, i.e., a weakly adsorbed carbon dioxide molecule, as shown in Figure 3c. Such ER and LHt low-temperature oxidation mechanisms were found by us (with similar energetics) for reactions on the gold cluster deposited on either a defect-free MgO (100) surface or one containing an FC, and both are expected to be relatively insensitive to the Au_n cluster size, correlating with the experimental results.

As aforementioned, the higher-temperature channel is strongly enhanced for Au_8 supported on a defect-rich MgO (100) support (compare the CO_2 signals at ~240 K in Figure 1a,b. This trend correlates with our simulations of a LH-periphery (LHp) reaction mechanism, starting with the CO adsorbed on the top-facet of the Au_8 cluster and the peroxo O_2* molecule bonded to the periphery of the interfacial layer of the cluster (see Figure 3f,g), where the distance between the C atom and the oxygen marked O_1 is $d(CO_1) = 4.49$ Å). Indeed, mapping of the potential energy surface along the $C-O_1$ reaction coordinate revealed for MgO (FC)/Au_8 a rather broad reaction barrier ΔE_b(LHp) ~ 0.5 eV (at d_b (CO_1) ~ 2.0 Å), while for the defect-free substrate a significantly higher barrier[23] was found, ΔE_b(LHp) ~ 0.8 eV; the reaction product is shown in Figure 3h for the MgO (FC)/Au_8 catalyst. Additionally, the availability of alternative cluster−periphery adsorption sites for the oxygen molecule, resulting in a distribution of distances between the adsorbed CO and the O_2* with a consequent distribution of reaction barriers, may underlie the observed relatively larger width of the higher temperature desorption peak (see Figure 1a).

Acknowledgment. Research at Georgia Tech is supported by the U.S. DOE, the AFOSR and the Academy of Finland, and at the University of Lausanne by the Swiss National Science Foundation. Simulations were performed on an IBM SP2 computer at the GIT Center for Computational Materials Science.

References and Notes

(1) (a) *Handbook of Heterogeneous Catalysis*; Ertl, G., Knözinger, H., Weitkamp, J., Eds.; Wiley: New York, 1997; 5 vols. (b) For a review of theoretical work on adsorption and reactions on metal surfaces see: Scheffler, M.; Stampfl, C. In *Handbook of Surface Science*, Vol. 2; Horn, K., Scheffler, M., Eds.; Elsevier: Amsterdam, 1999.

(2) Sault, A. G.; Madix, R. J.; Campbell, C. T. *Surf. Sci.* **1986**, *169*, 347; Saliba, N.; Parker, D. H.; Koel, B. E. *Surf. Sci.* **1998**, *410*, 270; Hammer, B.; Nørskov, J. K. *Nature* **1995**, *376*, 238.

(3) Haruta, M. *Catalysis Today* **1997**, *36*, 153; Haruta, M.; et al. *Chem. Express* **1988**, *5*, 349.

(4) Iizuka, Y; et al. *Catalysis Today* **1997**, *36*, 115.

(5) Grünwaldt, J. D.; Baiker, A. *J. Phys. Chem. B* **1999**, *103*, 1002.

(6) Valden, M.; Lai, X.; Goodman, D. W. *Science* **1998**, *281*, 1647.

(7) Heiz, U.; Vanolli, F.; Trento, L.; Schneider, W.-D. *Rev. Sci. Instrum.* **1997**, *68*, 1986.

(8) Cheng, H.-P.; Landman, U. *J. Phys. Chem.* **1994**, *98*, 3527.

(9) Bromann, K.; et al. *Science* **1996**, *274*, 956.

(10) Schaffner, M.-H.; Patthey, F.; Schneider, W.-D.; Pettersson, L. G. *Surf. Sci.* **1998**, *402−404*, 450.

(11) Heiz, U.; Vanolli, F.; Sanchez, A.; Schneider, W.-D. *J. Am. Chem. Soc.* **1998**, *120*, 9668.

(12) Heiz, U.; Sanchez, A.; Abbet, S.; Schneider, W.-D. *J. Am. Chem. Soc.* **1999**, *121*, 3214.

(13) Wu, M. C.; Corneille, J. S.; Estrada, C. A.; He, J.-W.; Goodman, D. W. *Chem. Phys. Lett.* **1991**, *182*, 472.

(14) Our temperature-programmed-desorption (TPD) setup is calibrated by using the known amount of CO desorbing from a Mo (100) surface (see Zaera, F.; Kollin, E.; Gland, J. L. *Chem. Phys. Lett.* **1985**, *12*, 464). By integrating the NO desorption peak and measuring the different detection efficiencies of NO and CO the amount of desorbing NO at 600 K can be estimated with an accuracy of 20%. Assuming that one NO molecule desorbs from each defect site the measured amount of NO gives the defect density,[7,11,12] and theoretically the obtained results can be explained by the presence of oxygen-vacancy F-centers (our calculated binding energy of NO to the perfect MgO (100) surface is 0.03 eV and is much higher, by at least an order of magnitude, for adsorption of the molecule in the vicinity of an F-center). Defect-rich films show typically around 1% ML of F-centers (see Figure 1d) whereas for the defect-poor films the number of defects is too small (<0.1% ML) to be measured with our experimental setup (see Figure 1e).

(15) The calculations were performed using the Born−Oppenheimer (BO) local-spin-density (LSD) molecular dynamics method (BO-LSD-MD, for details see ref 16, rewritten recently for massively parallel computing, and adapted in this study to deal with extended ionic surfaces as described below). The valence electrons of the Mg, O, C, and Au atoms (2, 6, 4, and 11 electrons, respectively) are described by norm-conserving non-local pseudopotentials (Troullier, N.; Martins, J. L. *Phys. Rev. B* **1991**, *43*, 1993), with a plane-wave basis set (kinetic energy cutoff of 62 Ry). The pseudopotentials[1] core radii (in units of a_o) are as follows (tilde indicates local component): Au: s̃ (2.50), p(3.00), d(2.00); C: s(1.50), p̃(1.54). Mg: s(2.50), p̃(2.75); O: s(1.45), p̃(1.45) with the Au pseudopotential treated relativistically (see Häkkinen, H.; Barnett, R. N.; Landman, U. *Phys. Rev. Lett.* **1999**, *82*, 3264). The MgO surface is constructed as follows (for a review of modeling of oxide surfaces, see Pacchioni, G. In *Chemisorption and Reactivity on Supported Clusters and Thin Films*; Lambert, R. M., Pacchioni, G., Eds.; Kluwer: Dordrecht, 1997; p 395): we treat "the active region" (i.e., the region surrounding the color center and/or beneath the Au cluster and adsorbed molecules) by the self-consistent Kohn−Sham formalism using the pseudopotentials described above for N_{AI} (ab initio) ions. We surround the outermost O ions further by "empty" (no valence electrons) N_{MgPP} Mg pseudopotentials and embed the system into a lattice of N_{PC} classical point charges of ± 2e located at the MgO lattice positions. Convergence of the total energy and electronic properties of the ab initio region are satisfactorily described by using $N_{PC} \sim 2000$. Furthermore, we have varied N_{AI} within the range $27 \leq N_{AI} \leq 107$ (with $N_{MgPP} \sim 50$) and found the color center (FC) formation energy (9.5 eV), KS eigenvalue of the FC state, and the binding energy of the Au_8 cluster to the defect-free MgO (100) surface and to the one containing an FC, to be rather insensitive (varying by no more than 5−10%) to N_{AI} within this range. Consequently, we have used the smallest ab initio slab for most of the calculations, particularly for mapping the activation barrier for the CO + O_2 reactions. It is generally accepted that while structural optimization with LSD yields reliable information, the binding energies are often overestimated. Such "overbinding" may be alleviated via the use of exchange-correlation (xc) gradient corrections (for the functionals used, see ref 16). Particularly pertinent to our study are such corrections to the calculated activation barriers of the ER, LHt, and LHp reaction mechanisms. Employing the post-GGA method (that is, calculating the gradient corrections using the Kohn−Sham orbitals and structures obtained in the LSD calculations[16]) we found that the values of the activation barriers were increased by no more than 0.1−0.2 eV. Moreover, neither the ordering of the barrier heights, nor any of the conclusions drawn in this study, are affected.

(16) Barnett, R. N.; Landman, U. *Phys. Rev. B* **1993**, *48*, 2081.

(17) For the MgO(FC)/Au_8 system (Figure 2a,b) the distance of the atoms from the surface plane of the MgO (100) surface are (the numbers of the Au atoms are the same as in Figure 2a,b): $d(1) = 5.14$ Å, $d(2) = d(2') = 4.34$ Å, $d(3) = d(3') = 2.64$ Å, $d(4) = d(4') = 2.17$ Å, and $d(5) = 1.54$ Å. For the MgO/Au_8 system all these distances are similar to the above (within 0.06 Å), except for the Au atom marked 5 for which $d(5) = 2.20$ Å.

(18) Cox, D. M.; Brickman, R. O.; Creegan, K.; Kaldor, A. *Mater. Res. Soc. Symp. Proc.* **1991**, *206*, 43; *Z. Phys. D* **1991**, *19*, 353. Recent

experiments revealed saturation coverage of one oxygen molecule for free Au_{2n}^- ($2 \leq n \leq 10$) clusters (Salisbury, B. E. Ph.D. Thesis, School of Physics, Georgia Institute of Technology, June 1999).

(19) The temperatures given here pertain to desorption of the final reaction product (CO_2), and they are not necessarily the temperatures at which the CO_2 is formed. The higher-temperature desorption peak may correspond to the periphery mechanism discussed at the end of the paper; however, it may also involve formation (at low temperature) of an adsorbed carbonate intermediate whose decomposition upon heating could result in a higher-temperature desorption peak of the CO_2 product. In this context we remark that from our experience the results shown here do not depend on the heating rate which we used (2 K/s), at least in the range of (2−20) K/s. Additionally, electron-stimulated processes can be safely excluded, as a biased skimmer with an orifice of 3 mm protects the sample from exposure to electrons.

(20) For recent theoretical studies of the adsorption of O_2, and CO oxidation, on Pt (111) see: (a) Eichler, A.; Hafner, J. *Phys. Rev. Lett.* **1997**, *79*, 4481; (b) *Phys. Rev. B* **1999**, *59*, 5960.

(21) We note here that while dissociative adsorption on free Au_8 and Au_8^- clusters is energetically favorable ($E_a = 1.10$ and 1.48 eV, respectively), requiring a sizeable free-energy barrier between the molecular and dissociated states ($\Delta E_b = 0.49$ eV for Au_8^- calculated at 300 K), dissociation of the oxygen molecule adsorbed on the MgO (FC)/Au_8 catalyst is endothermic (−0.72 eV), indicating that the catalytically activated species is indeed an adsorbed peroxo molecule. This finding is particularly interesting in light of the usual picture[1,20] of CO oxidation on extended surfaces of transition metals and coinage metals (other than gold) which involves dissociation of the adsorbed oxygen molecule prior to reaction.

(22) The gas-phase CO oxidation reaction while exothermic ($\Delta H^g_{calc} = 3.43$ eV, calculated at the post-GGA level and in agreement with ref 20b, $\Delta H^g_{expt} = 2.94$ eV), is hindered by a large activation barrier.

(23) The increased barrier can be traced to the above-noted higher adsorption energy of the O_2* molecule at the gold cluster interface for the defect-free MgO (100) surface.